ChemComm
Chemical Communications

Accepted Manuscript

This article can be cited before page numbers have been issued, to do this please use: U. Mall, R. J. Ortiz, I. B.M. Lozada, G. Williams and D. E. Herbert, *Chem. Commun.*, 2026, DOI: 10.1039/D6CC02913B.

ROYAL SOCIETY OF CHEMISTRY

rsc.li/chemcomm

ChemComm

View Article Online
DOI: 10.1039/D6CC02913B

COMMUNICATION

Highly Covalent, Pseudo-Octahedral Ru(II) Bis(amides): Panchromatic Absorption and Low-Energy Photocatalysis

Received 00th January 20xx,
Accepted 00th January 20xx

DOI: 10.1039/x0xx00000x

Utkarsh Mall,[a] Robert J. Ortiz,[a] Issiah B. Lozada,[a] J. A. Gareth Williams,[b] and David E. Herbert*[a]

A pseudo-octahedral Ru(II) complex supported by *trans*-amido donors is presented. Ru(t_{2g})-N(2p) dπ-pπ mixing generates highly covalent frontier MOs and strong absorption of visible/NIR light with π-anti-bonding-to-ligand charge-transfer character, covering a much wider range than is typical of Ru(II) chromophores. Low-energy irradiation generates a 33 ns dark excited-state capable of mediating electron- and energy-transfer photochemistry.

In photocatalysis, the ability to use low-energy excitation, notably red (600-700 nm) and near infrared (NIR) light, can circumvent issues with off-target reactivity,[1] light attenuation,[2] or complications with engineered solutions.[3] To achieve this, chromophores must be designed to absorb in this region of the electromagnetic spectrum and generate excited states with sufficiently long lifetimes and useful redox properties.[4] In addition to metalloporphyrins and emerging research into abundant-element coordination complexes,[5] heavier group 8 chromophores have arguably received the most attention in this area.[6] Low-energy photocatalysis with Os(II)[7] and Ru(II),[8] as well as Ir(III),[9] typically exploits the ability of heavier elements to undergo direct, spin-forbidden $S_0 \rightarrow T_1$ excitation thanks to large spin-orbit coupling (SOC), but these absorptions can be quite weak.[10] In comparison, low energy absorption with charge-transfer (CT) character should present higher absorptivity thanks to the nature of the transitions.[11] Panchromatic CT absorption is also coveted to enable low-energy light harvesting in dye-sensitized solar cells.[12,13]

Against this backdrop, we became interested in transition metal chromophores supported by anionic amido donors.[14] These offer a number of advantages: they can be installed via facile deprotonation of [N-H] units,[15] and the π-donor character emerging from the nitrogen-based lone pair increases the electron-richness of bound metal centres.[16] This proffers metal-to-ligand charge-transfer (MLCT) character to excited states in Co(III) bis(carbene)amido C^N^C complexes,[17] rare for Co(III). The redox-activity of amido donors also allows for multiple redox states of a Mn bis(amido).[18] As a π-donor ligand, amido moieties can also influence optical properties through orbital mixing. In (pseudo)octahedral complexes of electron-rich metals with occupied t_{2g}-type subsets, π-overlap with amido N(2p) orbitals reduces electron-electron repulsion within the metal's *d* orbitals. The 'nephelauxetic reduction'[19] resulting from covalent metal-amido bonds counteracts the weak-field nature of amido donors. This influences the excited-state landscape of d^3 Cr(III) chromophores, facilitating deep-red/NIR[20,21] and NIR-II luminescence.[22] M-N_{amido} mixing can also alter the nature of a molecule's absorption spectrum. For example, strong mixing between filled Fe(3d) and N_{amido}(2p) orbitals in d^6 Fe(II)[23] complexes supported by (4-phenanthridinyl-8-quinolinyl)amido ligands {(**L**)$_2$Fe; Fig. 1a} lends the highest occupied molecular orbitals Fe-N_{amido} π-antibonding character.[24] This results in 'π-antibonding-to-ligand' charge-transfer (PALCT) character[25] in the low energy absorption manifold (Fig. 1b) and broad, panchromatic absorption of visible light. Strong Fe-N_{amido} covalency, however, is insufficient to overcome the tendency of Fe(II) polypyridyls to rapidly populate metal-centred excited states despite the initial formation of CT ones.[26,27]

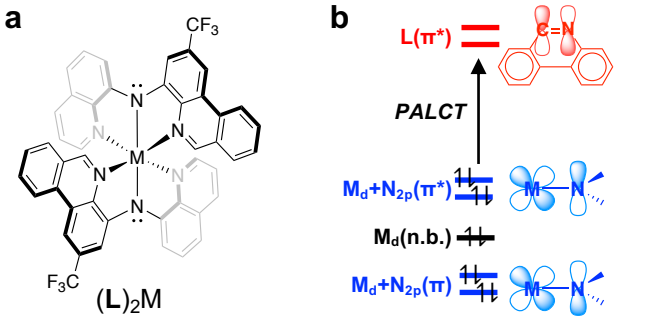

Fig. 1. (a) Pseudo-octahedral trans bis(amido) complexes (M = Fe[24]; M = Ru, this work) and (b) the 'π-antibonding-to-ligand' charge-transfer (PALCT) character of their lowest energy absorptions.

[a] Department of Chemistry, University of Manitoba, 144 Dysart Road, Winnipeg, Manitoba, R3T 2N2, Canada; *david.herbert@umanitoba.ca
[b] Department of Chemistry, Durham University, Durham, DH1 3LE, UK

We therefore turned our attention to Ru(II) complexes of chelating amido ligands to see if long-lived, reactive CT excited states could be accessed in heavier analogues of (**L**)$_2$Fe. Mono-amido Ru(II) complexes of deprotonated bis(8-quinolinyl)amine proligands[28] and *cis* bis(amido)Ru(IV) complexes using 2,3-diamino-2,3-dimethylbutane ligands have been reported,[29] but to our knowledge, Ru(II) complexes of *trans*-disposed bis(amido) donors have not been previously described. Heating a solution of the proligand **L**H with 0.5 equivalents of $(NH_3)_6RuCl_3$ and *N*-ethylmorpholine base in ethylene glycol afforded the cationic complex [(**L**)$_2$Ru]PF_6 as a dark red solid following metathesis with $KPF_{6(aq)}$ (Fig. 2a; 62% yield). [(**L**)$_2$Ru]PF_6 exhibits a broad, paramagnetically shifted ^{1}H NMR spectrum as expected of a formally d^5 species (Figure S1). Analysis by Evans' method gives a magnetic moment of 1.39 μ_B, consistent with a single unpaired electron and a low-spin d^5 configuration. [(**L**)$_2$Ru]$^+$ can be reduced at potentials accessible to common chemical reductants ($E_{1/2}$ = -0.60 V vs. ferrocene/ferrocenium ($FcH^{0/+}$), Fig. 2b) with a high degree of reversibility (i_{ox}/i_{red} = 0.91). Chemical reduction using cobaltocene in acetonitrile allowed for isolation of (**L**)$_2$Ru in 76% yield as a deep purple solid. Single crystals suitable for X-ray diffraction could be grown for both redox isomers (Fig. 2c and S2; Table S1). Comparing the two structures shows that, as with [(**L**)$_2$Fe]$^{0/+}$,[24] the Ru-N_{amido} bond distances decrease on oxidation. This is consistent with Ru-N_{amido} π-antibonding character in the HOMO of (**L**)$_2$Ru; as the orbital is depopulated, the Ru-N_{amido} bond order increases. The neutral species can be reduced at more cathodic potential ($E_{1/2}$ = -2.2 V), remarkably similar to the $E_{1/2}$ of [(**L**)$_2$Fe]$^{0/+}$,[24] while [(**L**)$_2$Ru]$^+$ can be further quasi-reversibly oxidized as well ($E_{1/2}$ = +0.054 V; i_{ox}/i_{red} = 1.48).

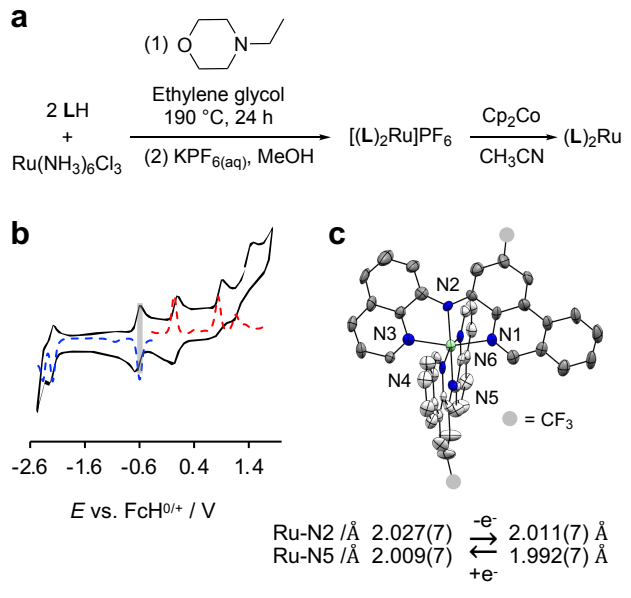

Fig. 2. (a) Synthesis of [(**L**)$_2$Ru]$^{0/+}$. (b) Cyclic voltammetry of [(**L**)$_2$Ru]PF_6 (solid black) overlaid with differential pulse voltammograms (dashed red/blue). The [(**L**)$_2$Ru]$^{+/0}$ couple is highlighted with a grey bar. (c) Solid-state structure of [(**L**)$_2$Ru], ellipsoids shown at 50% probability levels. Hydrogen atoms and CF_3 groups are omitted for clarity. The changes in d(Ru-N_{amido}) comparing the structures of [(**L**)$_2$Ru] and [(**L**)$_2$Ru]$^+$ (Fig. S2) are noted.

In 1st-row transition metal complexes (**L**)$_2$M (M = Fe, Co, Ni, Zn), the metal contribution to the HOMO is attenuated moving across the period, impacted by the relative energy of the metal's 3*d* valence orbitals.[25] Density functional theory (DFT) modelling shows that the mixing between filled metal t_{2g}-type orbitals and filled N_{amido}(2p), a prominent feature of (**L**)$_2$Fe,[23] is conserved in (**L**)$_2$Ru (Fig. 3a). The isosurfaces of the five highest-energy occupied orbitals present Ru-N_{amido} π-antibonding (HOMO, HOMO-1), Ru-based non-bonding character (HOMO-2), or Ru-N_{amido} π-bonding character (HOMO-3, HOMO-4). The lowest unoccupied molecular orbitals (LUMO, LUMO+1) present C=N π* character that is the hallmark of phenanthridine acceptors.[14] The absorption spectrum of (**L**)$_2$Ru is remarkably similar to that of (**L**)$_2$Fe (Fig. 3b), fully covering 300-800 nm. Electron-hole maps show the lowest energy absorptions result from the same PALCT character as for (**L**)$_2$Fe[25] (Fig. 3b, inset).

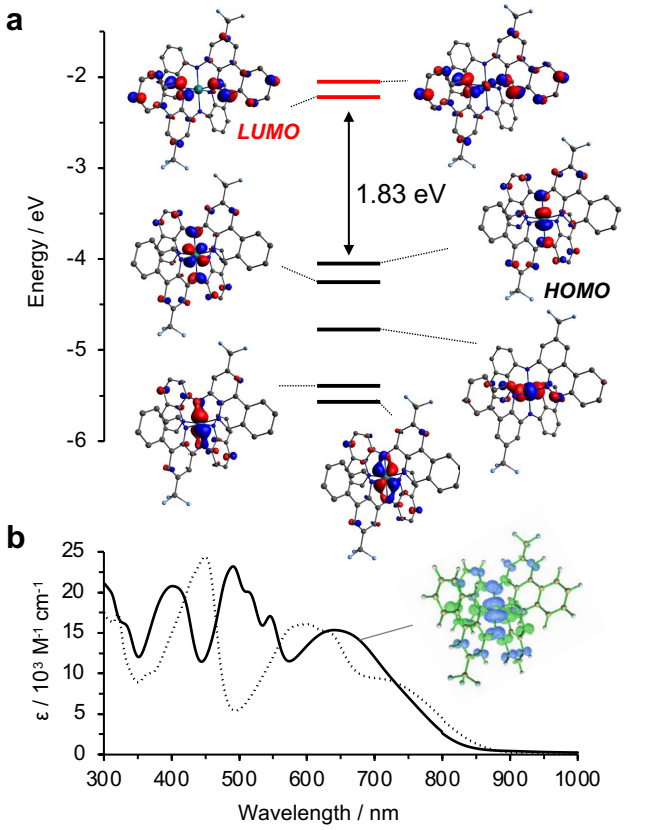

Fig. 3. (a) MO energy level diagram and selected orbital isosurfaces for (**L**)$_2$Ru. (b) UV-Vis absorption spectrum of (**L**)$_2$Ru (solid) and (**L**)$_2$Fe (dashed) in toluene. Inset: electron-hole map corresponding to the lowest energy manifold.

No evidence of emission from (**L**)$_2$Ru could be detected at room temperature in acetonitrile upon excitation into its low-energy band (λ_{ex} = 642 nm). A very weak signal in the NIR could be recorded in toluene, but too weak to determine the excited-state lifetime from its luminescence. In a frozen glass (77 K), a broad unstructured (and still quite weak) band is observed around 1000 nm tailing out to 1400 nm (Fig. S3; the short-wavelength onset of detector sensitivity is 950 nm). This emission provides an estimate of the excited state energy at ~1.3–1.4 eV (900–950 nm). DFT optimization of the lowest-

energy triplet excited state (T_1) is consistent with this estimate, suggesting $E(T_{1,DFT})$ = 1.28 eV. Spin-density plots (Fig. 4a and S4) show the T_1 hosts unpaired electron density on both metal and ligand, consistent with a ^{3}PALCT assignment. Optical transient absorption (oTA) measurements in toluene (λ_{ex} = 580 nm) confirmed the formation of a single, dominant excited state. A difference spectrum collected at a 15 ns delay (Fig. 4b) shows a prominent excited-state absorption (ESA) at 450 nm and weaker ESAs below ~350 nm and at ~570 nm. These sandwich three bleaches, with the two most prominent at ~500 nm and a broader one at ~650 nm. Most of these features can be faithfully reproduced by a linear combination of the absorption spectra of $[(\mathbf{L})_2Ru]^+$ and $[(\mathbf{L})_2Ru]^-$ (Fig. S5-S6), consistent with CT character to the excited state.[30] Single-wavelength kinetic traces focusing on the ESA (λ_{probe} = 430 nm; Fig. 4c) or bleach (650 nm; Fig. S8) could be fit with a monoexponential function, giving a lifetime of 32.8 ± 0.5 ns in toluene. The lifetime is solvent dependent; 18.3 ± 0.7 ns is measured in THF (Figs. S9 and S10). Despite the lifetime dependence on solvent dielectric, the absorption spectrum is not overly solvatochromic (Fig. S11).

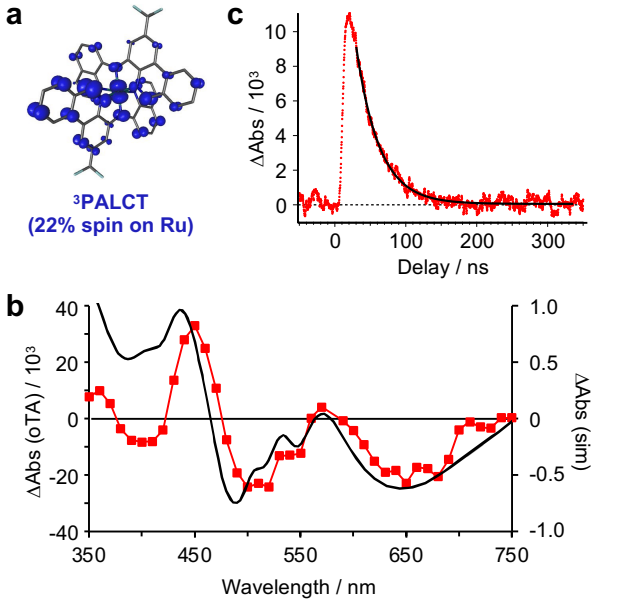

Fig. 4. (a) Spin-density map of the optimized triplet state of $(\mathbf{L})_2Ru$ (isosurface value = 0.004). (b) Full-spectrum oTA of $(\mathbf{L})_2Ru$ (λ_{pump} = 580 nm) in a toluene solution at a 15 ns delay in red overlaid with the spectroelectrochemical simulation of the PALCT state in black. (c) Kinetic trace from oTA experiment monitored at 430 nm (τ_{PALCT} = 32.8 ± 0.5 ns).

Lowering the temperature to 223 K, the lifetime in toluene extends to 42 ± 1 ns (Fig. S12). The variable-temperature lifetime data can be fit to the Arrhenius relation,[31,32] yielding an activation barrier for ground-state recovery of 1480 cm^{-1}; a frequency factor of 6.96 x 10^9 s^{-1}; and k_0 = 2.34 x 10^7 s^{-1} where k_0 is the temperature-independent rate. The activation barrier (E_a) is consistent with ground-state recovery mediated by thermal population of energetically close, but higher lying ^{3}MC states.[33–35] An E_a of 1480 cm^{-1} is not atypical of Ru(II) polypyridyl complexes with lower energy ^{3}MLCT excited states; it is higher than for $[Ru(bpy)_2(ppy)]^+$ analogues whose E_a values range from ~300-1000 cm^{-1},[36] but is low for most Ru polypyridyls, approaching instead values reported for strongly accepting ligands[37] and related heteroleptic complexes.[38]

With an excited state lifetime sufficient for bimolecular quenching, we evaluated the photocatalytic potential of $[(\mathbf{L})_2Ru]$ using low energy irradiation (740 nm LED; Fig. S13). At -0.60 V, the $[(\mathbf{L})_2Ru]^{0/+}$ reduction potential is relatively cathodic and consistent with an electron-rich metal centre, thanks to amido π-donation.[38] Using the computationally estimated $E(T_1)$, excited-state redox potentials of E^*_{ox} = -1.88 V and E^*_{red} = -0.91 V vs $FcH^{0/+}$ can be calculated. The ^{3}PALCT excited state of $(\mathbf{L})_2Ru$ should therefore be quite photoreducing compared to, for example, the dicationic $[Ru(bpy)_3]^{2+}$ (E^*_{ox} = -1.26 V vs $FcH^{0/+}$).[39,40] We thus first attempted the reduction of benzyl bromide (E_{red} = -1.7 V vs $FcH^{0/+}$)[41,42] in the presence of *N,N*-diisopropylethylamine and $(\mathbf{L})_2Ru$ (1-2 mol%), however no conversion was observed in C_6D_6 or THF. The reaction should be thermodynamically feasible; we attribute the lack of turnover to low cage-escape yields.[43] With the more easily reduced 4-nitrobenzyl bromide (E_{red} = -1.5 V vs $FcH^{0/+}$)[42,44], 10% conversion to a C-C coupled product was observed in acetonitrile after 48 h irradiation with red light, increasing to 49 ± 8% after 144 h (Fig. 5a). Comparable reactivity is observed with 650 nm illumination, consistent with both wavelengths accessing the same excited state in $(\mathbf{L})_2Ru$. In a less polar solvent (C_6D_6), catalytic turnover still occurs, but with only 5% conversion (27 h). In less polar solvents, the product of electron-transfer, $[(\mathbf{L})_2Ru]Br$, is insoluble and precipitates from the reaction medium, hampering turnover. Control reactions showed the necessity of both $(\mathbf{L})_2Ru$ and irradiation for catalysis.

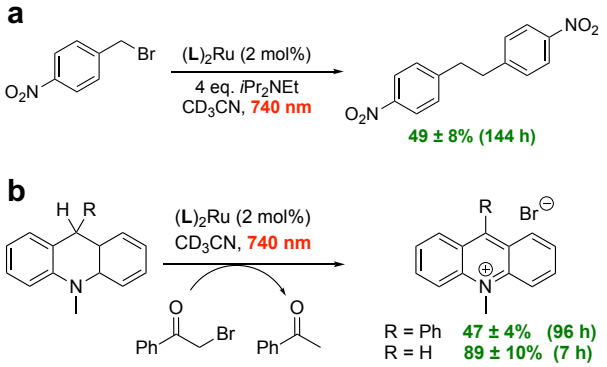

Fig. 5. Proof-of-principle photocatalytic reactions (a-c) performed using $(\mathbf{L})_2Ru$ and red light (740 nm) illumination.

We then examined the light-mediated hydrodehalogenation of phenacyl bromide (PB) using 10-methyl-9-phenyl-9,10-dihydroacridine (MPA; E_{ox} = +0.5 V vs $FcH^{0/+}$) as a hydride source (Fig. 5b). The parent 9,10-dihydro-10-methylacridine (DHA) can be photooxidized by $[Ru(bpy)_3]^{2+}$, but requires 450 nm light.[45,46] MPA is even more difficult to oxidize (E_{ox} = +0.4 V vs $FcH^{0/+}$). With $(\mathbf{L})_2Ru$, red light (740 nm) irradiation of a 2 mol% CD_3CN solution containing MPA (1 eq.), and PB (3 eq.) at 295 K led to clean consumption of MPA with formation of the acridinium salt (^{1}H NMR). Control reactions again proved the necessity of both light and $(\mathbf{L})_2Ru$. Given the relatively weak photooxidizing ability of the neutral $(\mathbf{L})_2Ru$ (E^*_{red} = -0.91 V vs

$FcH^{0/+}$), the reaction likely proceeds via initial electron transfer from $[(\mathbf{L})_2Ru]^*$ to PB, with turnover via MPA oxidation, to regenerate $(\mathbf{L})_2Ru$. Conversion reached 21% after 24 h, 37% after 72 h, and 47% after 96 h, reaching a maximum of 60% after 216 h. We attribute this deceleration (~0.9% h^{-1} during the first 24 h; ~0.1% h^{-1} over the final 96-216 h) to gradual photodegradation of $(\mathbf{L})_2Ru$ under prolonged irradiation.

Under otherwise identical conditions {2 mol% $(\mathbf{L})_2Ru$, 3 eq. phenacyl bromide, CD_3CN, 295 K, 740 nm} but using DHA which is 100 mV easier to oxidize than MPA, we see much faster DHA consumption (89% conversion after 7 h). A dark control reaction revealed that $(\mathbf{L})_2Ru$ mediates this transformation thermally, (54% conversion after 7 h in the absence of illumination). Experiments without added $(\mathbf{L})_2Ru$ showed no conversion. The light-driven reaction is accelerated relative to the thermal background, but the observed reactivity is not exclusively photochemical in origin. This stands in sharp contrast to the MPA reaction described above, for which no conversion was observed in the dark. We attribute the divergence to the difference in substrate oxidation potential: oxidation of DHA (+0.4 V) is accessible to $[(\mathbf{L})_2Ru]^+$ in its resting state, while MPA oxidation (+0.5 V) requires the more strongly oxidizing excited state generated by 740 nm excitation. The clean, light-exclusive reactivity with MPA provides the unambiguous demonstration of a rare example of deep red CT-mediated photocatalysis with Ru(II), with the DHA results marking the thermodynamic boundary at which the requirement for photoexcitation sets in. These proof-of-concept reactions highlight the utility of panchromatic-absorbing, neutral, reducing amido-metal complexes such as $(\mathbf{L})_2Ru$ in low-energy photocatalysis. Efforts to explore the full scope of the low-energy light photocatalytic potential of this class of chromophore are currently underway.

Author contributions

Conceptualization: UM, RJO, IBL, DEH. Formal analysis: UM, RJO, IBL, JAGW, DEH. Funding acquisition: DEH. Investigation: UM, RJO, IBL, JAGW. Supervision: DEH. Visualization: UM, RJO, JAGW, DEH. Writing – original draft: UM, RJO, DEH. Writing – review & editing: UM, RJO, JAGW, DEH.

Conflicts of interest

There are no conflicts to declare.

Data availability

The data and experimental details supporting this article have been included as part of the supplementary information (SI). Supplementary information: synthetic and photocatalytic protocols, computational data, NMR spectra, electrochemical plots, time-resolved spectroscopy data, crystal structure data, and further experimental details. The crystal structure data can also be obtained from the CCDC using deposition numbers 2553437 and 2553438. See DOI: .

Acknowledgements

View Article Online
DOI: 10.1039/D6CC02913B

Support for this work came from the Natural Sciences and Engineering Research Council of Canada (RGPIN-2022-04501 to DEH; CGS-D/Michael Smith Foreign Study Supplement to RJO), the Digital Research Alliance, and the Canada Foundation for Innovation and Research Manitoba for an award in support of an X-ray diffractometer (CFI #32146). We are also grateful to Prof. James K. McCusker for access to TA instrumentation, training, and insightful discussion, as well as to Bekah Bowers for assistant with TA measurements.

Notes and references

1 S. L. Goldschmid, N. E. Soon Tay, C. L. Joe, B. C. Lainhart, T. C. Sherwood, E. M. Simmons, M. Sezen-Edmonds and T. Rovis, *J. Am. Chem. Soc.*, 2022, **144**, 22409–22415.
2 K. C. Harper, E. G. Moschetta, S. V. Bordawekar and S. J. Wittenberger, *ACS Cent. Sci.*, 2019, **5**, 109–115.
3 L. Buglioni, F. Raymenants, A. Slattery, S. D. A. Zondag and T. Noël, *Chem. Rev.*, 2022, **122**, 2752–2906.
4 D. C. Cabanero and T. Rovis, *Nat. Rev. Chem.*, 2025, **9**, 28–45.
5 N. Kumar, T. Sharma, N. Thakur, R. Jain and N. Sinha, *Chem. - Eur. J.*, 2025, **31**, e202500365.
6 L. Fortier, C. Lefebvre and N. Hoffmann, *Beilstein J. Org. Chem.*, 2025, **21**, 296–326.
7 B. D. Ravetz, N. E. S. Tay, C. L. Joe, M. Sezen-Edmonds, M. A. Schmidt, Y. Tan, J. M. Janey, M. D. Eastgate and T. Rovis, *ACS Cent. Sci.*, 2020, **6**, 2053–2059.
8 G. Chacktas, B. Pfund, T. Kerackian, P. Yaltseva, M. Villeneuve, D. Durand, N. Fabre, C. Fiorini-Debuisschert, J.-C. Cintrat, O. S. Wenger and E. Romero, *ACS Catal.*, 2025, **15**, 13938–13947.
9 R. J. Ortiz, D. Nemez, M. Bhuiyan, K. A. Veilleux and D. E. Herbert, *Chem. Sci.*
10 M. Zhong and Y. Sun, *Chem. Catal.*, 2024, **4**, 100973.
11 D. Sorsche, M. A. L. Lima, N. Meitinger, K. Prasad, S. Mandal, K. D. Glusac, S. Rau and A. Pannwitz, *Coord. Chem. Rev.*, 2025, **530**, 216454.
12 M. K. Nazeeruddin, P. Péchy, T. Renouard, S. M. Zakeeruddin, R. Humphry-Baker, P. Comte, P. Liska, L. Cevey, E. Costa, V. Shklover, L. Spiccia, G. B. Deacon, C. A. Bignozzi and M. Grätzel, *J. Am. Chem. Soc.*, 2001, **123**, 1613–1624.
13 Q.-X. Zhou, W.-H. Lei, J.-R. Chen, C. Li, Y.-J. Hou, X.-S. Wang and B.-W. Zhang, *Chem. - Eur. J.*, 2010, **16**, 3157–3165.
14 D. E. Herbert, *Can. J. Chem.*, 2023, **101**, 892–902.
15 P. Mandapati, P. K. Giesbrecht, R. L. Davis and D. E. Herbert, *Inorg. Chem.*, 2017, **56**, 3674–3685.
16 P. Mandapati, J. D. Braun, I. B. Lozada, J. A. G. Williams and D. E. Herbert, *Inorg. Chem.*, 2020, **59**, 12504–12517.
17 N. Sinha, B. Pfund, C. Wegeberg, A. Prescimone and O. S. Wenger, *J. Am. Chem. Soc.*, 2022, **144**, 9859–9873.
18 B. Wittwer, N. Dickmann, S. Berg, D. Leitner, L. Tesi, D. Hunger, R. Gratzl, J. Van Slageren, N. I. Neuman, D. Munz and S. Hohloch, *Chem. Commun.*, 2022, **58**, 6096–6099.
19 N. Sinha, P. Yaltseva and O. S. Wenger, *Angew. Chem., Int. Ed.*, 2023, **62**, e202303864.
20 N. Sawicka, C. J. Craze, P. N. Horton, S. J. Coles, E. Richards and S. J. A. Pope, *Chem. Commun.*, 2022, **58**, 5733–5736.
21 Y. Cheng, Q. Yang, J. He, W. Zou, K. Liao, X. Chang, C. Zou and W. Lu, *Dalton Trans.*, 2023, **52**, 2561–2565.

View Article Online
DOI: 10.1039/D6CC02913B

22 N. Sinha, J.-R. Jiménez, B. Pfund, A. Prescimone, C. Piguet and O. S. Wenger, *Angew. Chem., Int. Ed.*, 2021, **60**, 23722–23728.
23 C. B. Larsen, J. D. Braun, I. B. Lozada, K. Kunnus, E. Biasin, C. Kolodziej, C. Burda, A. A. Cordones, K. J. Gaffney and D. E. Herbert, *J. Am. Chem. Soc.*, 2021, **143**, 20645–20656.
24 J. D. Braun, I. B. Lozada, C. Kolodziej, C. Burda, K. M. E. Newman, J. van Lierop, R. L. Davis and D. E. Herbert, *Nat. Chem.*, 2019, **11**, 1144–1150.
25 J. D. Braun, I. B. Lozada and D. E. Herbert, *Inorg. Chem.*, 2020, **59**, 17746–17757.
26 M. E. Reinhard, B. K. Sidhu, I. B. Lozada, N. Powers-Riggs, R. J. Ortiz, H. Lim, R. Nickel, J. van Lierop, R. Alonso-Mori, M. Chollet, L. B. Gee, P. L. Kramer, T. Kroll, S. L. Raj, T. B. van Driel, A. A. Cordones, D. Sokaras, D. E. Herbert and K. J. Gaffney, *J. Am. Chem. Soc.*, 2024, **146**, 17908–17916.
27 C. Wegeberg, B. K. Sidhu, P. Chábera, J. Uhlig, R. A. Cowin, J. A. Weinstein, P. Persson, A. Yartsev and D. E. Herbert, *Chem. Sci.*, 2026, **17**, 6125–6137.
28 T. A. Betley, B. A. Qian and J. C. Peters, *Inorg. Chem.*, 2008, **47**, 11570–11582.
29 W.-H. Chiu, S.-M. Peng and C.-M. Che, *Inorg. Chem.*, 1996, **35**, 3369–3374.
30 A. M. Brown, C. E. McCusker and J. K. McCusker, *Dalton Trans.*, 2014, **43**, 17635–17646.
31 J. K. McCusker, H. Toftlund, A. L. Rheingold and D. N. Hendrickson, *J. Am. Chem. Soc.*, 1993, **115**, 1797–1804.
32 S. J. Steinke, E. J. Piechota, L. M. Loftus and C. Turro, *J. Am. Chem. Soc.*, 2022, **144**, 20177–20182.
33 J. Van Houten and R. J. Watts, *J. Am. Chem. Soc.*, 1976, **98**, 4853–4858.
34 N. H. Damrauer, G. Cerullo, A. Yeh, T. R. Boussie, C. V. Shank and J. K. McCusker, *Science*, 1997, **275**, 54–57.
35 T. C. Motley, L. Troian-Gautier, M. K. Brennaman and G. J. Meyer, *Inorg. Chem.*, 2017, **56**, 13579–13592.
36 T. C. Motley, L. Troian-Gautier, M. K. Brennaman and G. J. Meyer, *Inorg. Chem.*, 2017, **56**, 13579–13592.
37 G. H. Allen, R. P. White, D. P. Rillema and T. J. Meyer, *J. Am. Chem. Soc.*, 1984, **106**, 2613–2620.
38 P. Mandapati, J. D. Braun, C. Killeen, R. L. Davis, J. A. G. Williams and D. E. Herbert, *Inorg. Chem.*, 2019, **58**, 14808–14817.
39 C. R. Bock, J. A. Connor, A. R. Gutierrez, T. J. Meyer, D. G. Whitten, B. P. Sullivan and J. K. Nagle, *J. Am. Chem. Soc.*, 1979, **101**, 4815–4824.
40 F. Glaser, S. De Kreijger, K. Achilleos, L. N. Satheesh, A. Ripak, N. Chantry, C. Bourgois, S. Quiquempoix, J. Scriven, J. Rubens, M. Vander Wee-Léonard, M. Daenen, M. Gillard, B. Elias and L. Troian-Gautier, *ChemPhotoChem*, 2024, **8**, e202400134.
41 D. Ravelli, S. Protti and M. Fagnoni, *Chem. Rev.*, 2016, **116**, 9850–9913.
42 Potentials vs SCE were converted to $FcH^{0/+}$ according to: V. V. Pavlishchuk and A. W. Addison, *Inorg. Chim. Acta*, 2000, **298**, 97–102.
43 M. J. Goodwin, J. C. Dickenson, A. Ripak, A. M. Deetz, J. S. McCarthy, G. J. Meyer and L. Troian-Gautier, *Chem. Rev.*, 2024, **124**, 7379–7464.
44 J. G. Lawless, D. E. Bartak and M. D. Hawley, *J. Am. Chem. Soc.*, 1969, **91**, 7121–7127.
45 S. Fukuzumi, S. Mochizuki and T. Tanaka, *J. Phys. Chem.*, 1990, **94**, 722–726.
46 C. K. Prier, D. A. Rankic and D. W. C. MacMillan, *Chem. Rev.*, 2013, **113**, 5322–5363.

View Article Online
DOI: 10.1039/D6CC02913B

Data Availability Statement

The data supporting this article have been included as part of the supplementary information (SI).

Supplementary information: supporting computational data, NMR spectra, electrochemical plots, time-resolved spectroscopy data, crystal structure data, and further experimental details.

The crystal structure data can also be obtained from the CCDC using deposition numbers 2553437 and 2553438.